On the importance of wave-like structures in the occurrence of equatorial plasma bubbles: A case study

V. Lakshmi Narayanan,[1] A. Taori,[2] A. K. Patra,[2] K. Emperumal,[1] and S. Gurubaran[1]

Received 4 August 2011; revised 19 October 2011; accepted 11 November 2011; published 10 January 2012.

[1] Coordinated observations of equatorial plasma bubbles (EPBs) have been made with an all-sky airglow imager, narrow bandwidth photometer, VHF radar, and ionosonde over the Indian sector on the night of 23 March 2009. The prereversal enhancement (PRE) in the vertical plasma drift during the postsunset hours on this day was moderate. Range type spread *F* was found to occur immediately after the satellite traces were noted in the ionograms. This was well recorded in measurements made by all-sky imager, narrow band photometer, and VHF radar. The airglow emission intensities also revealed the presence of a large-scale wave-like structure (LSWS) together with the plasma bubbles that coincided with plume structures observed in the VHF radar echoes. The periodicity of the occurrence of bubbles (and plumes) and their interdepletion distances suggest the presence of small-scale wave-like structures (SSWS) on this night. The results are compared with the ionosonde observations made on the night of 21 February 2008. The PRE and the maximum height attained by the *F* layer were very similar to that of 23 March 2009. In addition, the ionograms showed the presence of satellite traces. However, no subsequent evolution of spread *F* was noticed. Considering the satellite traces to have their origin in LSWS, these observations imply that though the presence of LSWS is important for the triggering of EPBs, they alone are not sufficient. However, the coexistence of both LSWS and SSWS may have the potential to trigger EPBs.

Citation: Narayanan, V. L., A. Taori, A. K. Patra, K. Emperumal, and S. Gurubaran (2012), On the importance of wave-like structures in the occurrence of equatorial plasma bubbles: A case study, *J. Geophys. Res.*, *117*, A01306, doi:10.1029/2011JA017054.

1. Introduction

[2] The postsunset equatorial ionosphere is prone to generation of plasma instabilities leading to formation of plasma density irregularities that affect radio wave propagation and navigation systems. Lack of plasma production immediately after sunset combined with higher recombination in the *E* region of the ionosphere results in a steep gradient in electron density. Further, during the evening hours, the *F* layer often rises because of an increased eastward electric field known as the prereversal enhancement (PRE) [*Woodman*, 2009; *Abdu et al.*, 2009]. One of the dramatic manifestations of this postsunset ionospheric electrodynamics is the appearance of irregularities that cause VHF backscattering in the *F* region. These vertically extended structures are a manifestation of equatorial spread *F* (ESF) [*Woodman and LaHoz*, 1976] and often termed as plasma plumes in radar maps and equatorial plasma bubbles (EPBs) in optical imagers. They are believed to originate from field-aligned irregularities in the equatorial *F* region, with the Generalized Rayleigh Taylor (GRT) instability as the often attributed mechanism responsible for them [*Kelley*, 1989]. The growth rate of GRT instability is inversely proportional to the ion-neutral collision frequency and hence the higher the *F* region base height, the greater the probability of occurrence of ESF (or EPBs). PRE is believed to be an important factor in the generation of GRT instability as it lifts up the *F* region in the evening hours. In addition to the PRE, a perturbation is a necessary requirement for the initiation of GRT instability. There had been several reports suggesting that the atmospheric gravity waves reaching ionospheric altitudes from below provide this much needed seed [e.g., *Kelley et al.*, 1981; *Taori et al.*, 2010]. Recently, there had been interesting reports suggesting that large-scale wave-like structures (LSWS) are present in the bottom side of the *F* region prior to the onset of EPBs [*Tsunoda*, 2005, 2008; *Thampi et al.*, 2009]. However, there is still a lack of a comprehensive understanding of the underlying processes responsible for the triggering of EPBs. As a result the day-to-day variability in the occurrence of ESF remains to be an intriguing phenomenon.

[1]Equatorial Geophysical Research Laboratory, Indian Institute of Geomagnetism, Tirunelveli, India.
[2]National Atmospheric Research Laboratory, Gadanki, India.

0148-0227/12/2011JA017054

[3] In this work we present two cases in which LSWS were noted and the *F* layer height (h′*F*) over the magnetic equator was below 330 km around sunset hours. However, only in one case EPBs occurred and their signatures were observed by VHF radar, ionosonde and optical instruments, whereas in the other case no ESF was observed. In the former case the measured interdepletion distances (in airglow imaging) and the temporal spacing between successive plumes (in VHF radar and airglow photometry) suggest existence of short-period, small-scale wave-like (SSWS) structures overriding LSWS. We characterize the observed structures in EPBs with the aid of simultaneous airglow, radar and ionosonde measurements and discuss the role of LSWS and SSWS in the occurrence of EPBs.

2. Observations

2.1. Ionosonde

[4] A vertical incidence Canadian Advanced Digital Ionosonde (CADI) was operated from Tirunelveli (8.7°N, 77.8°E, geographic; 1.1°N dip latitude). Being a dip equatorial station, measurements made by Tirunelveli ionosonde complement the airglow and VHF radar observations made at Gadanki (13.5°N, 79.2°E, geographic; 6.5°N dip latitude).

2.2. VHF Radar

[5] The VHF radar operated at Gadanki is a high-power coherent pulsed radar. It operates at 53 MHz with maximum power aperture product $\sim 3 \times 10^{10}$ Wm^2. The radar system consists of 1024 Yagi antennas arranged in two orthogonal sets, 32 high-power transmitters, 32 units of transmitter receiver duplexers and a phase coherent receiver. A detailed description of various subsystems [*Rao et al.*, 1995] and the observation of ESF irregularities using this radar were reported earlier [*Patra et al.*, 1995, 1997]. To obtain strong echoes from field-aligned ESF irregularities, the radar beam was oriented at 14.8°N from zenith to make it perpendicular to the north-south geomagnetic field lines.

2.3. Airglow Instruments

2.3.1. All-Sky Airglow Imager

[6] The all-sky airglow imager of the Indian Institute of Geomagnetism used in this campaign was designed for *f* /4 optics and was equipped with a six position filter wheel. One of the interference filters was a 2 nm bandwidth filter centered at 630.0 nm for the observation of the O(^{1}D) emission from thermosphere. The sensor was a back illuminated CCD array of 512 × 512 pixels with high quantum efficiency (>90%) in the wavelength region of interest. Further details of the instrument and image processing methods to retrieve information are discussed in the work of *Narayanan et al.* [2009b]. The instrument had been successfully utilized for studies of mesospheric wave motions [*Narayanan et al.*, 2009a, 2010]. Though the imager is capable of making observations with a FOV greater than 170°, we had physically reduced the FOV to ∼120° in order to avoid spurious vehicular light disturbances from the nearby highway. The observed 630.0 nm images were projected onto a latitude-longitude grid assuming an emission altitude of 250 km before evaluating the parameters of the observed depletion structures. The zenith horizontal resolution of the imager at 250 km height was ∼2 km. This instrument was operated from Gadanki during March 2009. Regular operations are being carried out from Tirunelveli.

2.3.2. Narrow Field-of-View Photometer

[7] The Mesosphere-Lower Thermosphere Photometer (MLTP), developed at National Atmospheric Research Laboratory, Gadanki, utilizes a narrow bandwidth (FWHM ∼0.4 nm) interference filter with center wavelength at 630.0 nm for monitoring thermospheric O(^{1}D) emission. The filter has ∼60% transmission at 24°C. The temperature of the filter is controlled with a precision of better than 0.25°C by a set of 16 Peltier elements and a proportional integral derivative (PID) controller. The MLTP uses three *f* / 2 lens systems for collimating the incoming radiation and refocusing the image on to the detector with a slit to limit the full field-of-view (FOV) to 4°. The MLTP has a Hamamatsu R943–02 photomultiplier tube with a GaAs(Cs) photocathode with wide spectral response (160–930 nm), low dark count (20 counts s^{-1} at –20°C) and high quantum efficiency (∼14% at 630 nm). The MLTP was pointed toward zenith and signals were integrated for 10 s duration. First results and validation of MLTP results were discussed by *Taori et al.* [2011].

3. Results and Discussion

[8] The observations reported in this work were made on the nights of 23 March 2009 and 21 February 2008. It may be noted that on 21 February 2008 only ionosonde observations from Tirunelveli were made use of. Since the day was near to the full moon period, no optical observations were carried out. Further, the VHF radar was not operated on this night. We have selected 21 February 2008 for comparison from ionogram database covering ∼3 years because of the similarities in the ionospheric conditions before the onset of ESF. Further, there was presence of satellite traces on both the days.

[9] The observations correspond to magnetically quiet days during low sunspot years. All of the 3 hourly k_p values on these days were less than 3 and A_p was 2 for 23 March 2009 and 6 for 21 February 2008.

[10] The temporal variations in the base height (*h′F*) of the *F* region over Tirunelveli on these nights are shown in Figure 1. The dotted lines represent the height variations during the presence of ESF. It may be noted that the maximum height of the *F* layer was around 330 km on both the days. Since the ionosonde is located at a dip equatorial station, the rise of the *F* layer can be attributed only to the PRE. Meridional winds and diffusion do not play any role in raising the height of *F* layer over the magnetic equator [e.g., *Krishna Murthy et al.*, 1990]. It may be noted that the PRE was moderate and similar on both the days under consideration.

[11] Figure 2a shows a set of ionograms recorded from the dip equatorial station, Tirunelveli, on the night of 23 March 2009. It reveals a satellite trace at 20:40 Indian Standard Time (IST). It is believed that the satellite traces indicate the presence of obliquely tilted layers and such traces are often found just prior to the onset of range type ESF [*Lyon et al.*, 1961; *Rastogi*, 1977; *Abdu et al.*, 1981; *Tsunoda*, 2008; *Takahashi et al.*, 2010]. Such tilted layers are evidence for the existence of large-scale structures in ionization and can be taken as a signature of LSWS at the *F* region heights.

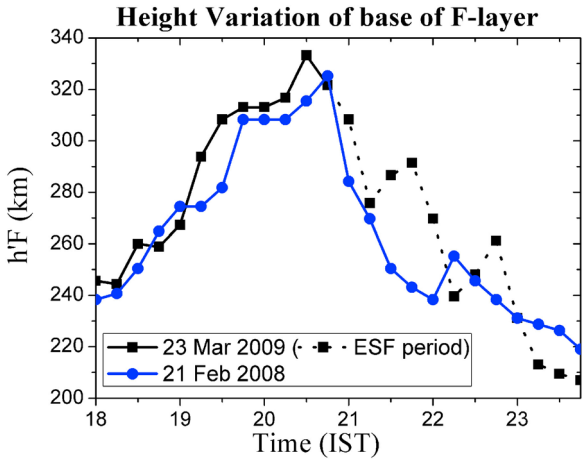

Figure 1. Variations of base height of the *F* region (h′*F*) over Tirunelveli on 23 March 2009 and 21 February 2008. The dotted lines represent the height variations during the presence of ESF.

Range type ESF was noticed to occur by 20:50 IST, immediately after the formation of satellite traces. Later, we will show that the ESF was well recorded in optical and radar remote sensing carried out from Gadanki.

[12] Figure 2b shows sample of the ionograms from Tirunelveli recorded on the night of 21 February 2008. It may be noted that there was a satellite trace in the first multiple reflection (i.e., second *F* trace) of ionogram recorded at 19:30 IST. By 20:15 IST, the satellite trace is noticeable in the primary *F* trace itself. However, no subsequent evolution of ESF was noticed on this day. Therefore, the ionosonde observations on 21 February 2008 suggest that the existence of LSWS (satellite trace) is not sufficient enough to trigger ESF on this night.

[13] Figures 3a and 3b show the range-time-intensity (RTI) and range-time-velocity (RTV) plots, respectively, obtained from the VHF radar observations on the night of 23 March 2009. From about 20:30 IST, the radar echoes were confined to an altitude range of 200–270 km. After 21:45 IST, one notices vertically elongated shapes in the radar echoes signifying the presence of strong patches of field-aligned plasma irregularities. Noteworthy was the occurrence of plasma plume structures with temporal spacing of ∼20 min. As the plumes go higher, they tend to get tilted. Such tilted structures are often attributed to the vertical shears in the *F* region drift velocity [*Zalesak et al.*, 1982]. Further, the radar echoes were centered around 250 km, and therefore, the signatures of these plumes would have a one-to-one imprint in airglow intensity. It may also be noted that the radar maps reveal the presence of echoes around 150 km during 20:00–23:00 IST. The vertical Doppler velocities shown in Figure 3b indicate alternate upward and downward drifts in the 150 km echoes at these times suggesting the presence of wave-like motion.

[14] Figures 4a–4p show a time sequence of selected OI 630.0 nm images for the night of 23 March 2009 (Note that we have not removed the Van Rhijn contribution in the images as it only introduces a near-linear trend in the image data at zenith angles close to horizon). Two groups of bubbles were observed on this night comprising a series of five bubbles in the first group and three in the second. First group was observed between ∼21:30 and ∼22:50 IST and the second one between ∼22:40 IST and ∼23:30 IST (the time when the observations were interrupted by clouds). These bubbles were found drifting eastward. The interdepletion distances and the drift speeds of the bubbles are tabulated in Table 1. The parameters for the first bubble in group 1 could not be calculated as tracking its motion was difficult. Both the interdepletion distances and drift velocities were relatively higher for the first group compared to the second (see Table 1). The spatial separation between the two groups is estimated to be ∼400 km and there was an enhanced intensity region between them (see Figures 4k–4m). Further, the first two bubbles (bubbles 6 and 7) in the second group appear to have merged to one as time passed by. From Table 1, a reduction in the eastward drift speed of the bubbles with time may be noted. Such a reduction in drift speed with time is well reported in the literature [e.g., *Kumar et al.*, 1995; *Mendillo et al.*, 1997; *Kishore and Mukherjee*, 2007].

[15] To estimate the temporal separation between the observed bubbles, the ratios of average interdepletion distances and average drift velocities for both groups of bubbles were calculated separately. The ratio gives a temporal separation of ∼18 min for both groups. This is in close agreement with the temporal spacing of these features inferred from the VHF radar and MLTP observations that will be discussed later. These observations suggest the presence of a SSWS with a time period of ∼18 min.

[16] It may be noted from Figure 3 that the bases of plumes in radar echoes were confined to times prior to 22:45 IST corresponding to the passage of the first group of bubbles observed by the imager over zenith (see Figure 4k). It may be recalled that the VHF radar beam was pointed orthogonal to the geomagnetic field and intersects the latter at 14.8°N geographic latitude. The imaging observations indicate that the second group of bubbles traversing from the west might have reached the longitude of VHF radar only after 23:35 IST. Further, it may be noticed that those bubbles did not extend up to 14.8° during that time (see Figure 4p). The absence of irregularities in the region where the radar beam was pointed was probably the reason why the radar did not detect any plumes during the passage of second group of bubbles.

[17] Figure 5 shows the east-west cross sections taken from the selected images depicted in Figure 4. The cross sections were detrended for any linear variations. The plot reveals important information that could not have been easily obtained from a visual inspection of the images. In Figures 5a–5e, a large-scale intensity variation in 630.0 nm emission, herein interpreted as LSWS, with a wavelength in the range 450–500 km, may be noticed. The reduced intensity region analogous to the trough of this wave-like feature is expected to occur when the bottom side *F* region moves upward. Within about next 10–15 min, few narrower wave-like fluctuations formed within the trough of the LSWS. Comparison with Figure 4 clarifies that the narrower structures correspond to the bubble features noted in the images. Interestingly, the ionosonde measurements of base height of *F* layer (Figure 1) showed an upward movement during 21:00–21:30 IST coinciding with the formation of the first group of bubbles. This lends credence to our inference that

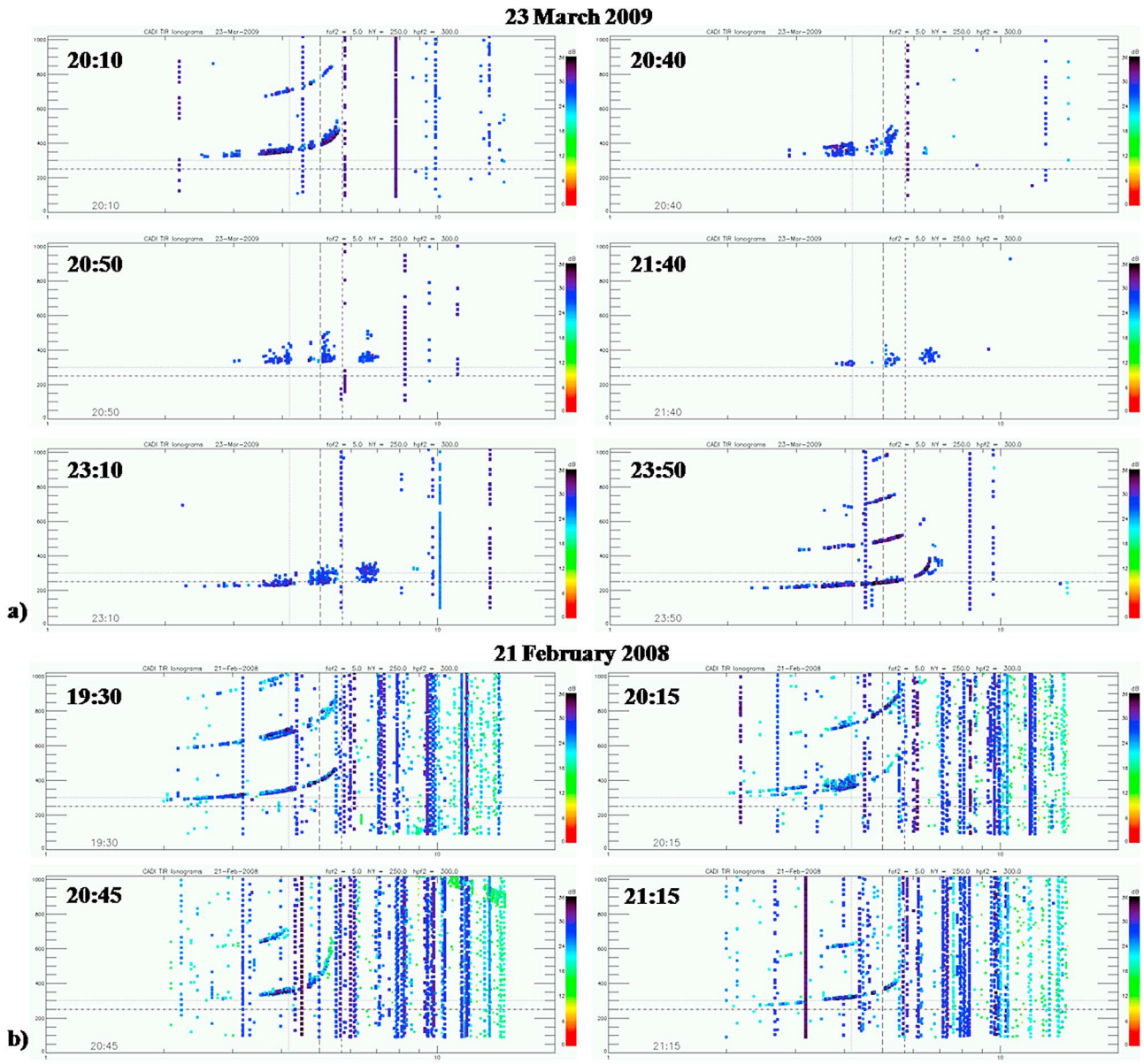

Figure 2. Ionograms recorded from the equatorial station Tirunelveli on the nights of (a) 23 March 2009 and (b) 21 February 2008. Times are in IST (UT + 5.5 h). The vertical lines are noise.

the reduced intensity region might be due to the upward movement of the *F* region.

[18] Following the passage of the first group of bubbles, an enhancement in emission intensity started to appear in the west (Figure 5f). From Figures 5j–5m, it may be inferred that this region of intensity enhancement had a zonal extent of about 350–400 km. This would correspond to the downward motion of the bottom side *F* region associated with the crest of the LSWS. Noteworthy is the fact that the plasma bubble formation was inhibited during this period. Immediately after this intensity enhancement region passed by, a second group of bubbles was observed. Height variations of the base height of the *F* layer depicted in Figure 1 shows that there was another upward movement between 22:15 and 22:45 IST. The second group of bubbles might have been associated with this upward perturbation of the *F* region. It may be noticed that the second group of bubbles were entering into the FOV of the imager around 22:40 IST rather than forming within the FOV (Figures 4 and 5). It may also be observed from Figure 5 that the LSWS drifted eastward along with the bubbles. Another important aspect that can be noted by comparing the extracted cross sections with the images is that the LSWS was meridionally extended (see Figure 4a). Airglow observations could not be carried out after 23:30 IST owing to clouds.

[19] In Figure 4, we also noted a north-south movement of an east-west-aligned belt of enhanced intensity region. At first sight, this might appear like the southward movement of equatorial ionization anomaly (EIA) crest associated with the reverse fountain. It may be mentioned that the FOV of our imager covers ~2.5°–10.5° N dip latitudes. An earlier study by *Wiens et al.* [2004] showed that the southward

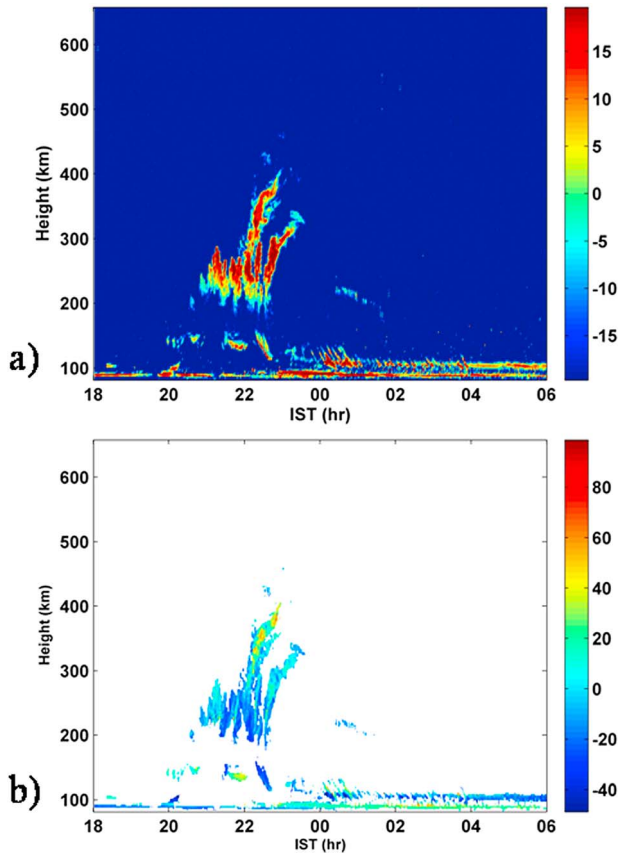

Figure 3. VHF radar observations for 23 March 2009: (a) range-time-intensity and (b) range-time-velocity.

movement of the EIA crest region typically reaches only up to 9° magnetic latitudes. Therefore, it was unlikely that the observed zonal belt of enhanced intensity was due to the passage of EIA crest. Further, the deduced phase speed of this enhanced intensity region was ∼100 m s^{-1}, which was nearly twice of that reported for the equatorward movement of the EIA crest [*King*, 1968; *Kulkarni*, 1975; *Sridharan et al.*, 1993; *Mukherjee*, 2002]. It is quite possible that the east-west-aligned enhanced band was linked with TID. We, however, are not sure about it since we have no way to know its wavelength as we have never observed two intense bands in any of the images.

[20] This belt of enhanced intensity region does not appear to play any important role in the triggering of the observed bubbles as the first group of bubbles had started to originate before the intense region crossed the FOV. Further, we have observed a reduction in the altitudinal extent (directly associated with the latitudinal extent seen in images) of the second group of bubbles. It is quite possible that the plasma filling of the depleted flux tubes from the enhanced intensity region might have been responsible for this reduction in the growth of second group of bubbles. Since the focus of this study is on the triggering of the EPBs, we conclude that the north-south intensity movement did not play any noticeable role in the generation of the observed bubbles, though they would have a possible effect on the suppression of the bubbles.

[21] It may be noted that this north-south intensity movement is different from the observed signature of the LSWS we are discussing here. Especially, an ambiguity arises in the later periods of observation when the brightening owing to the passage of east-west-aligned enhanced intensity region adds to the enhancement corresponding to the LSWS (see Figures 4l–4p). One may infer from Figures 4a–4c and 4h–4k that there was a meridionally extended enhanced intensity region on both the sides of the first group of bubbles that formed within a meridionally extended large-scale reduced intensity region. Moreover, Figures 5h–5l show that the intensity enhancement associated with the LSWS drifted eastward along with the bubbles. It is worth mentioning that the presence of LSWS is also inferred from satellite traces in the ionograms.

[22] The 630.0 nm zenith intensity variations observed by MLTP on the night of 23 March 2009 are depicted in Figure 6. One may notice a decrease in the 630.0 nm intensity from ∼20:00 to 21:30 IST. After 22:00 IST, the intensity exhibited an increase till 23:00 IST followed by subsequent decrease till midnight. The sharp bite-outs noticed in 630 nm nightglow intensity are an indication of the plasma bubbles. Narrow-angle photometric observations provide the time series that are useful in the study of wave motions. It may be noted that the zenith intensity variations observed between 20:00 to 21:30 IST might also have contribution from reduction of ion production after sunset. Any large-scale wave motion might be superposed on such variations, thereby making it difficult to isolate the contribution of the particular wave from narrow angle photometric observations. It may be noted that all the bubbles observed in imaging observations were not readily seen in MLTP observations. However, MLTP observations clearly show presence of bubbles 3 and 4 seen in images (see Figure 6). The temporal separation between the occurrences of the bubbles was ∼20 min in concurrence with the temporal separation of VHF radar plumes and that inferred from the all-sky imager.

[23] While the studies on gravity wave seeding of the EPBs have been made over a few decades, the discussions on the possibility of wave-wave interactions in bringing about EPBs are limited in the literature. *Sekar et al.* [2001] discuss such a possibility of triggering of EPBs by means of interaction of two long-wavelength modes. They found that the relative strength of small-scale disturbance need not be very high, if the large-scale wave motion is of sufficient amplitude and the mechanism is a viable one especially in triggering low-level plasma plumes resulting in bottom type ESF irregularities. The observations reported herein suggest that the LSWS brings the conditions favorable for the generation of the instabilities while the triggering is due to the passage of SSWS.

[24] Already, the importance of PRE and LSWS in determining the day-to-day variability of EPBs is discussed in literature [e.g., *Abdu et al.*, 2009; *Tsunoda*, 2005]. Many of the past studies involving airglow imaging observations showed that the inter depletion distances of the EPBs lie in the range of 50 to 250 km. This falls below the typical scale sizes reported for LSWS. However, the mechanism of breaking of postsunset vortex giving rise to the EPBs [*Kudeki and Bhattacharyya*, 1999] could not explain the formation of late night EPBs. The present case study highlights the

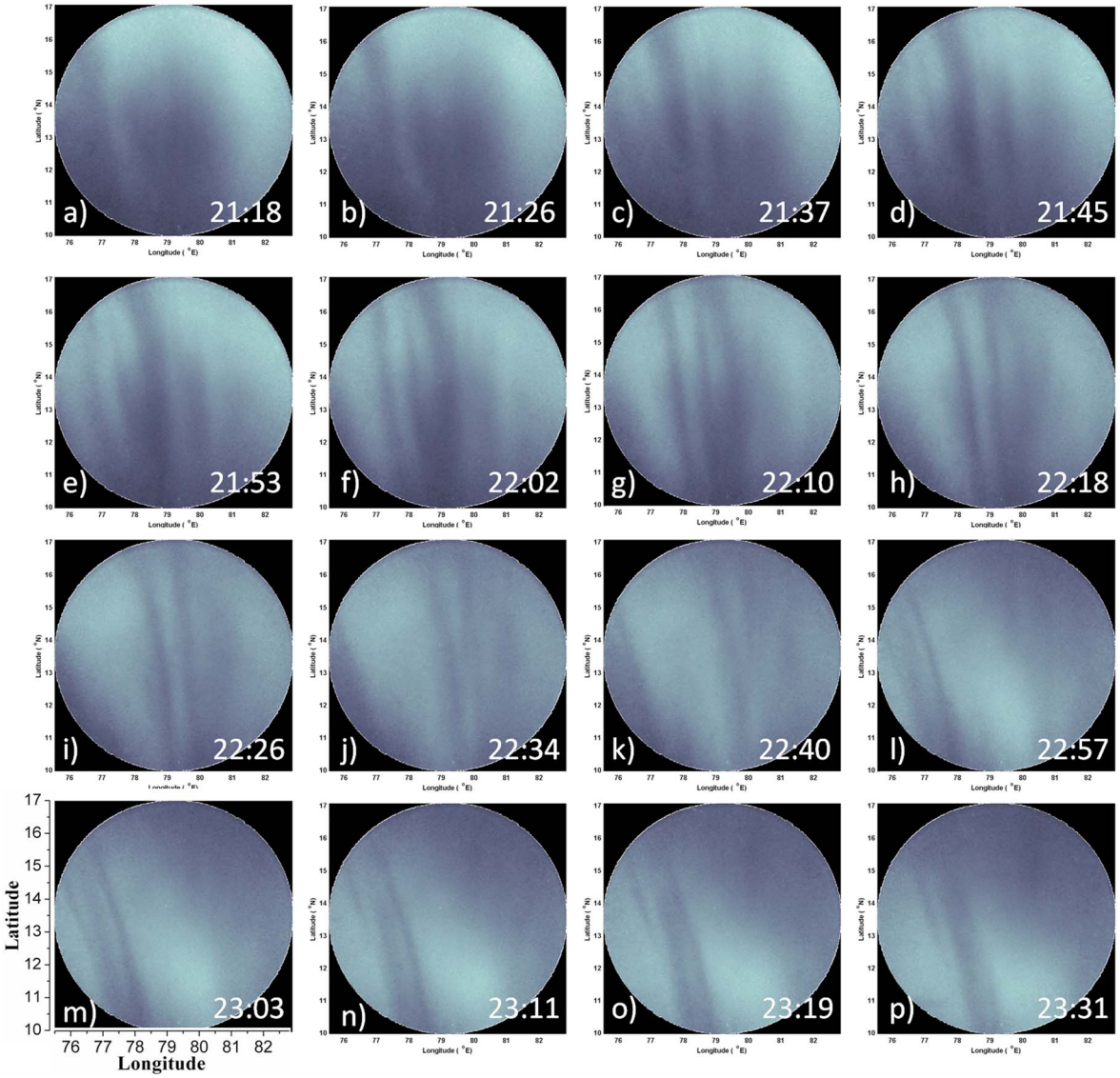

Figure 4. Selected all-sky images taken from Gadanki showing plasma bubbles observed on the night of 23 March 2009. Times are in IST.

role of SSWS in addition to the LSWS and PRE in bringing about the EPBs. Conceptually, the triggering of EPBs by means of interaction of large- and small-scale wave modes

Table 1. Measured Parameters of Observed Plasma Bubbles on 23 March 2009[a]

Bubble Number	Drift Velocity (m s^{-1})	Interdepletion Distance (km)
	Set 1	
1	NA	—
2	97 ± 25	NA
3	125 ± 19	107 (between 2 and 3)
4	87 ± 29	127 (between 3 and 4)
5	109 ± 13	98 (between 4 and 5)
	Set 2	
6	75 ± 12	—
7	68 ± 21	70 (between 6 and 7)
8	51 ± 17	67 (between 7 and 8)

[a]NA, not available.

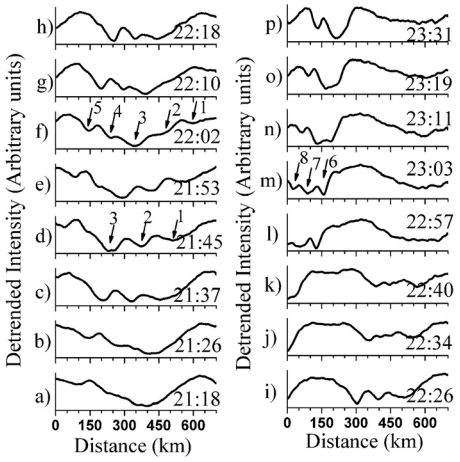

Figure 5. East-west cross sections passing through the zenith of the observation location (Gadanki) extracted from the images shown in Figure 4. Times are in IST.

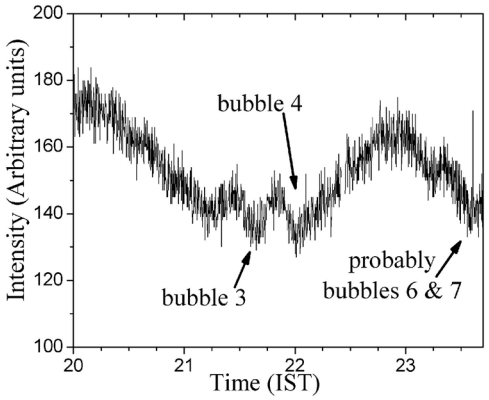

Figure 6. MLTP observation of OI 630 nm emission on the night of 23 March 2009, indicating the occurrence of depleted regions in the nocturnal intensity variability.

is a potential mechanism that may even explain the formation of late night bubbles. However, the source of the SSWS and the relative importance of LSWS and SSWS needs to be addressed in future studies with a larger database.

4. Summary and Conclusion

[25] The ionospheric measurements showed that the *F* layer height rise was similar and not significant on both the nights considered here indicating insignificant role of PRE. Satellite traces were observed in both cases in ionograms implying the presence of LSWS on both the nights.

[26] The inference from all-sky imaging on 23 March 2009 that the observed bubbles evolve within a region of large-scale depletion indicates that instabilities arise from the regions of upward moving plasma. This view is supported by the ionosonde measurements of h′*F* as well. Noteworthy is the observation that no bubbles evolved in the downward moving enhanced intensity regions associated with the LSWS. Here, we find the wavelength of the LSWS was ~400 km or greater. The evolution of the individual plasma bubbles with interdepletion distances around 100 km might be the result of seeding by relatively smaller-scale wave motions. Thus, the interactions between large- and small-scale waves occurring in the bottom side *F* region appear to have triggered the EPBs that occurred on 23 March 2009. Another noticeable revelation from the all-sky images is that the observed LSWS is predominantly zonal in nature (i.e., its structure is meridionally extended).

[27] On 21 February 2008, only a satellite trace was noticed in ionograms from Tirunelveli without subsequent evolution into ESF. Therefore, a comparison of the observations on these two days suggest that in the absence of significant PRE (as the *F* layer height rise was moderate and very similar), the presence of both LSWS and SSWS might be important in bringing about an EPB and only presence of LSWS may not be sufficient for the same. This, however, needs to be ascertained with a larger database of similar nature than that used in the present study. We would like to address this issue in our future investigation with a larger database.

[28] **Acknowledgments.** V.L.N. thanks the director of the Indian Institute of Geomagnetism for a research fellowship. This work is supported by the Department of Science and Technology and Department of Space, Government of India. The present study was undertaken as one of the CAWSES-India Phase-II Theme-3 (Atmospheric Coupling Processes) initiatives.

[29] Robert Lysak thanks the reviewers for their assistance in evaluating this paper.

References

Abdu, M. A., I. S. Batista, and J. A. Bittencourt (1981), Some characteristics of spread *F* at the magnetic equatorial station Fortaleza, *J. Geophys. Res.*, *86*, 6836–6842, doi:10.1029/JA086iA08p06836.

Abdu, M. A., I. S. Batista, B. W. Reinisch, J. R. de Souza, J. H. A. Sobral, T. R. Pedersen, A. F. Medeiros, N. J. Schuch, E. R. de Paula, and K. M. Groves (2009), Conjugate Point Equatorial Experiment (COPEX) campaign in Brazil: Electrodynamics highlights on spread *F* development conditions and day-to-day variability, *J. Geophys. Res.*, *114*, A04308, doi:10.1029/2008JA013749.

Kelley, M. C. (1989), *The Earth's Ionosphere: Plasma Physics and Electrodynamics*, Academic, San Diego, Calif.

Kelley, M. C., M. F. Larsen, and C. LaHoz (1981), Gravity wave initiation of equatorial spread *F*: A case study, *J. Geophys. Res.*, *86*, 9087–9100, doi:10.1029/JA086iA11p09087.

King, J. W. (1968), Airglow observations and the decay of the ionospheric equatorial anomaly, *J. Atmos. Terr. Phys.*, *30*, 391–402, doi:10.1016/0021-9169(68)90110-4.

Kishore, M. H., and G. K. Mukherjee (2007), Equatorial *F* region plasma drifts: A study using OI 630 nm emission all-sky images, *Curr. Sci.*, *93*, 488–497.

Krishna Murthy, B. V., S. S. Hari, and V. V. Somayajulu (1990), Nighttime equatorial thermospheric meridional winds from ionospheric *h'F* data, *J. Geophys. Res.*, *95*, 4307–4310, doi:10.1029/JA095iA04p04307.

Kudeki, E., and S. Bhattacharyya (1999), Postsunset vortex in equatorial *F* region plasma drifts and implications for bottomside spread *F*, *J. Geophys. Res.*, *104*, 28,163–28,170, doi:10.1029/1998JA900111.

Kulkarni, P. V. (1975), 6300Å night airglow and the geomagnetic control of the equatorial anomaly, *Proc. Indiana Acad. Sci.*, *82*, 46–54.

Kumar, S., A. K. Gwal, B. M. Pathan, and D. R. K. Rao (1995), Zonal drifts of ionospheric irregularities at temperate latitude in the Indian region, *Ann. Geophys.*, *13*, 724–729, doi:10.1007/s00585-995-0724-5.

Lyon, A. J., N. J. Skinner, and R. W. Wright (1961), Equatorial spread *F* at Ibadan, Nigeria, *J. Atmos. Terr. Phys.*, *21*, 100–119, doi:10.1016/0021-9169(61)90104-0.

Mendillo, M., J. Baumgardner, M. Colerico, and D. Nottingham (1997), Imaging science contributions to equatorial aeronomy: Initial results from MISETA program, *J. Atmos. Sol. Terr. Phys.*, *59*, 1587–1599, doi:10.1016/S1364-6826(96)00158-7.

Mukherjee, G. K. (2002), Mapping of the simultaneous movement of the equatorial ionization anomaly (EIA) and ionospheric plasma bubbles through all-sky imaging of OI 630 nm emission, *Terr. Atmos. Ocean. Sci.*, *13*, 53–64.

Narayanan, V. L., S. Gurubaran, and K. Emperumal (2009a), A case study of a mesospheric bore event observed with an all-sky airglow imager at Tirunelveli (8.7°N), *J. Geophys. Res.*, *114*, D08114, doi:10.1029/2008JD010602.

Narayanan, V. L., S. Gurubaran, and K. Emperumal (2009b), Imaging observations of upper mesospheric nightglow emissions from Tirunelveli (8.7°N), *Indian J. Radio Space Phys.*, *38*, 150–158.

Narayanan, V. L., S. Gurubaran, and K. Emperumal (2010), Airglow imaging observations of small-scale structures driven by convective instability in the upper mesosphere over Tirunelveli (8.7°N), *J. Geophys. Res.*, *115*, D19119, doi:10.1029/2009JD012937.

Patra, A. K., V. K. Anandan, P. B. Rao, and A. R. Jain (1995), First observations of equatorial spread *F* from Indian MST radar, *Radio Sci.*, *30*, 1159–1165, doi:10.1029/95RS00650.

Patra, A. K., P. B. Rao, V. K. Anandan, and A. R. Jain (1997), Radar observations of 2.8m equatorial spread-*F* irregularities, *J. Atmos. Sol. Terr. Phys.*, *59*, 1633–1641, doi:10.1016/S1364-6826(96)00162-9.

Rao, P. B., A. R. Jain, P. Kishore, P. Balamuralidhar, S. H. Damle, and G. Viswanathan (1995), Indian MST radar: 1. System description and sample vector wind measurements in ST mode, *Radio Sci.*, *30*, 1125–1138, doi:10.1029/95RS00787.

Rastogi, R. G. (1977), Equatorial range spread *F* and high multiple echoes from the *F* region, *Proc. Indian Acad. Sci.*, *85*, 230–235.

Sekar, R., E. A. Kherani, P. B. Rao, and A. K. Patra (2001), Interaction of two long-wavelength modes in the nonlinear numerical simulation of

equatorial spread *F*, *J. Geophys. Res.*, *106*, 24,765–24,775, doi:10.1029/2000JA000361.

Sridharan, R., R. Sekar, and S. Gurubaran (1993), Two-dimensional high-resolution imaging of the equatorial plasma fountain, *J. Atmos. Terr. Phys.*, *55*, 1661–1665, doi:10.1016/0021-9169(93)90170-4.

Takahashi, H., et al. (2010), Equatorial ionosphere bottom-type spread *F* observed by OI 630.0 nm airglow imaging, *Geophys. Res. Lett.*, *37*, L03102, doi:10.1029/2009GL041802.

Taori, A., J. J. Makela, and M. Taylor (2010), Mesospheric wave signatures and equatorial plasma bubbles: A case study, *J. Geophys. Res.*, *115*, A06302, doi:10.1029/2009JA015088.

Taori, A., N. Dashora, K. Raghunath, J. M. Russell III, and M. G. Mlynczak (2011), Simultaneous mesosphere-thermosphere-ionosphere parameter measurements over Gadanki (13.5°N, 79.2°E): First results, *J. Geophys. Res.*, *116*, A07308, doi:10.1029/2010JA016154.

Thampi, S. V., M. Yamamoto, R. T. Tsunoda, Y. Otsuka, T. Tsugawa, J. Uemoto, and M. Ishii (2009), First observations of large-scale wave structure and equatorial spread *F* using CERTO radio beacon on the C/NOFS satellite, *Geophys. Res. Lett.*, *36*, L18111, doi:10.1029/2009GL039887.

Tsunoda, R. T. (2005), On the enigma of day-to-day variability in equatorial spread *F*, *Geophys. Res. Lett.*, *32*, L08103, doi:10.1029/2005GL022512.

Tsunoda, R. T. (2008), Satellite traces: An ionogram signature for large-scale wave structure and a precursor for equatorial spread *F*, *Geophys. Res. Lett.*, *35*, L20110, doi:10.1029/2008GL035706.

Wiens, R. H., S. Habtemichael, F. Andemariam, K. Welday, J. Criswick, S. Brown, and S. Sargoytchev (2004), Brightness variations of the northern 630 nm intertropical arc and the midnight pressure bulge over Eritrea, *Ann. Geophys.*, *22*, 3251–3259, doi:10.5194/angeo-22-3251-2004.

Woodman, R. F. (2009), Spread *F*—An old equatorial aeronomy problem finally resolved?, *Ann. Geophys.*, *27*, 1915–1934, doi:10.5194/angeo-27-1915-2009.

Woodman, R. F., and C. LaHoz (1976), Radar observations of *F* region equatorial irregularities, *J. Geophys. Res.*, *81*, 5447–5466, doi:10.1029/JA081i031p05447.

Zalesak, S. T., S. L. Ossakow, and P. K. Chaturvedi (1982), Nonlinear equatorial spread *F*: The effect of neutral winds and background Pedersen conductivity, *J. Geophys. Res.*, *87*, 151–166, doi:10.1029/JA087iA01p00151.

K. Emperumal, S. Gurubaran, and V. L. Narayanan, Equatorial Geophysical Research Laboratory, Indian Institute of Geomagnetism, Krisnapuram, Tirunelveli, Tamilnadu 627011, India. (narayananvlwins@gmail.com)

A. K. Patra and A. Taori, National Atmospheric Research Laboratory, Pakala Mandal, Gadanki, Andhra Pradesh 517112, India.